

Supporting Information:

Kinetic H₂S/CO₂ Selectivity in an Exceptionally Sterically Hindered Amine Membrane

Shraavya Rao ^[1], Xuepeng Deng ^[1], Changlong Zou ^[1], Babul Prasad ^[1,2], Yang Han ^[1], Li-Chiang Lin ^[1,3] and W.S. Winston Ho*^[1,4]

^[1] *William G. Lowrie Department of Chemical and Biomolecular Engineering, The Ohio State University, 151 West Woodruff Avenue, Columbus, OH 43210-1350, USA.*

^[2] *Polymer Science and Engineering Division, CSIR-National Chemical Laboratory, Dr. Homi Bhabha Road, Pashan, Pune 411008, India.*

^[3] *Department of Chemical Engineering, National Taiwan University, Taipei 10617, Taiwan*

^[4] *Department of Materials Science and Engineering, The Ohio State University, 2041 College Road, Columbus, OH 43210-1178, USA.*

* Corresponding author. Tel.: +1 614 292 9970; fax: +1 614 292 3769.

E-mail address: ho.192@osu.edu (W.S.W. Ho)

Contents

S1. Materials and Methods	3
S2. Supporting Results.....	10
S3. Carrier Structures and Properties.....	12
S4. Thickness-dependence of H ₂ S Permeability	13
S5. Facilitated Transport Model	16
S6. H ₂ S/CO ₂ Upper Bounds and Literature Data	21
S7. References	24

S1. Materials and Methods

S1.1. Materials

Poly(vinyl alcohol) (PVA) POVAL 100-88 (94%, 87 – 89% hydrolysis degree) was provided by Kuraray America. Glacial acetic acid, potassium hydroxide (KOH), glycine, sodium hydroxide (NaOH), and glutaraldehyde (50% in water) were purchased from Sigma Aldrich. 2-Amino-2-methylpropan-1-ol was purchased from VWR Chemicals. Deuterium oxide (99.9% atom D, containing 0.05% wt.% sodium salt of 3-(trimethylsilyl)propionic-2,2,3,3-d₄ acid (TMSP)) was bought from Sigma Aldrich. Methanol, acetone, chloroform, and ethanol were acquired from Fisher Scientific.

Purolite® A600OH strong base anion-exchange resin and Purolite® C100H acid cation-exchange resin were provided by Purolite Corporation. Nanoporous polysulfone with an average pore size of 10 nm and a porosity of 7% was purchased from Mann+Hummel. The feed gases, CO₂ and H₂S, and the helium required for the gas chromatograph (GC) were purchased from Linde.

S1.2. Carrier synthesis

Glycine was used as received without further purification. It was reacted with KOH stoichiometrically to form potassium glycinate (Gly) during membrane preparation.

N-(1,1-dimethyl-2-hydroxyethyl)-aminoisobutyric acid was synthesized via the Bargellini reaction ^[1]. The details of the reaction have been covered in literature ^[2]. 2-Amino-2-methylpropan-1-ol (1 eq), chloroform (2 eq) and acetone (10 eq) were added to a round bottom flask under stirring with the temperature controlled at 0°C with an ethanol-water ice bath. Powdered NaOH (5 eq) was added to the solution under nitrogen in 5 portions while keeping the temperature below 5°C. The solution was stirred under nitrogen and allowed to reach room

temperature overnight. The slurry obtained was filtered under vacuum and the filtrate collected. The solid residue was once again filtered with 100 ml of methanol. The combined filtrate was subjected to ion-exchange using Purolite® C100H to remove NaOH. The solution was then evaporated under vacuum, and the solid product obtained was washed with acetone. The product thus obtained contained some inorganic impurities, which were removed by once again dissolving the solid in ethanol. The insoluble impurity was filtered off, and the soluble product was obtained by vacuum distillation. The product, *N*-(1,1-dimethyl-2-hydroxyethyl)-aminoisobutyric acid, was collected as an off-white solid. ¹H NMR (D₂O): δ (ppm) = 3.56 (s, 2H), 1.59 (s, 6H), 1.37 (s, 6H); ¹³C NMR (D₂O): δ (ppm) = 177.3 (1C), 67.4 (1C), 63.6 (1C), 62.2 (1C), 24.4 (2C), 20.9 (2C).

For ¹H NMR, samples were prepared by dissolving the product in D₂O to form a 1 wt.% solution. The D₂O contained 0.05 wt.% TMS as a standard. *N*-(1,1-dimethyl-2-hydroxyethyl)-aminoisobutyric acid was reacted with KOH stoichiometrically to form potassium *N*-(1,1-dimethyl-2-hydroxyethyl)-aminoisobutyrate (TB-AIBA) during membrane preparation.

In this study, potassium glycinate and potassium TB-AIBA were chosen as model compounds to represent unhindered and highly sterically hindered amines, respectively. For the synthesis of amine compounds with intermediate steric hindrance, the readers are referred to our previous work [3].

SI.3. Crosslinking of PVA

PVA (1 equivalent) was dissolved in water overnight to obtain a 4 wt.% solution. Glutaraldehyde (0.25 equivalent) was added to the solution as a crosslinker. A drop of glacial acetic acid was added to catalyze the crosslinking. The crosslinking reaction was conducted overnight at 35°C, after which a significant increase in the viscosity was observed. The acetic

acid was removed using Purolite® A600OH strong base anion-exchange resin.

SI.4. Membrane preparation

A 5 wt.% carrier solution was prepared by dissolving the amino acid carrier in water. A stoichiometric amount of KOH was added under stirring to deprotonate the amino acid. The coating solution was prepared by adding the carrier solution dropwise to 4 wt.% crosslinked PVA under vigorous stirring. The solution composition was controlled to ensure a carrier content of 70 wt.% in the dry membrane, based on our prior work optimizing H₂S/CO₂ separation performance with carrier contents between 60 wt.% and 80 wt.% [3]. After centrifuging at 3000 rpm for 5 min, the solution was coated on to a nanoporous polysulfone support with a GARDCO adjustable micrometer film applicator (Paul N. Gardner Company). The membrane was dried in a fume hood for 30 min and then cured at 120°C for 6 hours to complete the crosslinking. The thickness of the facilitated transport membrane (FTM) was measured using a Mitutoyo electronic indicator (Model 543-252B, Mitutoyo America Corp., Aurora, IL) with an accuracy of ±0.5 µm. Unless otherwise specified, the selective layer thickness was controlled at 3 µm.

For attenuated total reflection (ATR) Fourier transform infrared (FTIR) characterization, freestanding films were prepared by coating the solution onto a glass plate. The films were dried in a fume hood and then cured at 120°C for 6 h. For the in-situ experiments, the films were first dried in a fume hood overnight and then transferred onto KBr pellets for the curing.

SI.5. Material characterization

Carrier purities were confirmed using ¹H NMR. All ¹H NMR experiments were conducted using a Bruker Avance III 400 instrument.

The quantitative ¹³C NMR spectra were conducted on a Bruker Avance III HD Ascend 600 MHz instrument using the inverse gated proton decoupling method with TopSpin version 3.6

software. 64 scans were collected for each spectrum. The spectra were obtained with a pulse interval of 76 s, which was five times longer than the longest T1 for the carbon peaks of the CO₂-sorbed carrier samples to minimize the nuclear Overhauser effect (NOE).

For the CO₂ loading experiments, 0.5 M carrier solutions of potassium glycinate (Gly) and potassium *N*-(1,1-dimethyl-2-hydroxyethyl)-aminoisobutyrate (TB-AIBA) were prepared by dissolving the carrier in D₂O along with a stoichiometric amount of KOH. The solutions were loaded with CO₂ by bubbling pure CO₂ through a syringe needle at a flow rate of 1.5 cm³ (STP)/min. The CO₂ loading was estimated by measuring the weight increase, and then further confirmed by the ¹³C NMR spectra.

To confirm incorporation of the carrier, the membranes were examined using X-ray photoelectron spectroscopy (XPS). The spectra were collected by a ThermoFisher Nexsa G2 XPS, equipped with a monochromatic (Al) X-ray gun.

The membrane samples were also analyzed using ATR-FTIR spectroscopy using a Nexus 470 FTIR spectrometer (Nicolet Instruments Co., Waltham, MA). 64 scans were collected with a resolution of 4 cm⁻¹ and averaged for each spectrum.

In-situ FTIR experiments were conducted on the same instrument using a transmission reaction cell equipped with KBr plates [4]. The cell was wrapped with heating tape to control the temperature at 110°C. The gas was introduced into the cell at a flow rate of 10 cm³ (STP)/min. Before entering the cell, the gas was humidified at 22°C. The background spectrum was collected using humidified N₂, after which the gas was switched to 20% CO₂ in N₂. The samples were exposed to the gas for at least 4 h before the spectrum was collected. 64 scans were collected and averaged for each spectrum.

The cross-sectional thickness was confirmed using scanning electron microscopy (SEM, FEI

Apreeo LoVac, Thermo Fisher Scientific Inc., Waltham, MA).

A Wicke-Kallenbach permeation apparatus was used to measure the membrane transport performance. A detailed description of the setup can be found in a previous publication [5]. For convenience, a brief summary is provided below. The membrane was placed in a gas permeation cell with an area of 2.7 cm² for testing. The feed and sweep gases passed through stainless-steel packed column humidifiers, before entering the permeation cell in countercurrent fashion. The feed and sweep relative humidities (RHs) were maintained by water injection through two HPLC pumps (Varian ProStar, Model 210, Varian Inc., Palo Alto, CA), respectively. The exit gases from the permeation cells passed through stainless-steel water knockouts before entering the GC. The GC (Model 6890 N, Agilent Technologies), equipped with a micropacked column (80/100 Hayesep-D, Sigma-Aldrich) and a thermal conductivity detector (TCD), was used to analyze the concentrations of CO₂ and H₂S.

The membranes were tested at 107°C and 7 bar feed pressure. For examining the effect of membrane thickness on selectivity, a feed gas composition of 99% CO₂ and 1.0% H₂S was used before humidification. The feed side was maintained at 100% RH, while the sweep water content was controlled at 85%, based on recommendations from prior publications [6,7]. For investigating the dependence of H₂S permeance on feed H₂S concentration, the feed H₂S concentration was varied between 0.5 – 30% (dry basis), with the balance being CO₂. The gas permeances and selectivity were calculated using Equations (1) – (3):

$$P_{H_2S} = \frac{J_{H_2S}}{\frac{\Delta p_{feed, H_2S} - \Delta p_{ret, H_2S}}{\ln \left(\frac{\Delta p_{feed, H_2S}}{\Delta p_{ret, H_2S}} \right)}} \quad (1)$$

$$P_{CO_2} = \frac{J_{CO_2}}{\frac{\Delta p_{feed, CO_2} - \Delta p_{ret, CO_2}}{\ln(\Delta p_{feed, CO_2} / \Delta p_{ret, CO_2})}} \quad (2)$$

$$\alpha = \frac{P_{H_2S}}{P_{CO_2}} \quad (3)$$

where P_{H_2S} and P_{CO_2} denote the H₂S and CO₂ permeances, respectively, J_{H_2S} and J_{CO_2} the H₂S and CO₂ fluxes, respectively, and $\Delta p_{feed,i}$ and $\Delta p_{ret,i}$ the transmembrane partial pressure differentials at the feed inlet and retentate outlet for gas i , respectively. The uncertainty in the H₂S permeance was calculated to be ~8% based on an error propagation analysis [8].

The selection of feed gas composition, feed pressure, and operating temperature was guided by practical considerations for the selective removal of H₂S from CO₂. For further details and their practical relevance to acid gas separations, we refer readers to our previous work [3].

SI.6. Computational

Density functional theory (DFT) calculations were conducted as per the procedure described by Deng et al [9]. In brief, the calculations used a combination of the B3LYP (Becke three-parameter Lee–Yang–Parr) functional along with the 6-311++G(d,p) basis set, and were implemented in Gaussian 16. Geometry optimization and frequency analysis were conducted for each structure, i.e., the reactants, complexes, transition-state structures, and products, to identify its thermodynamically favorable geometry, and the corresponding electronic energy and frequencies. For reactants, complexes, and products, the optimization was continued until no imaginary frequency was found; for transition-state structures, the optimization was conducted until only one imaginary frequency existed. In order to account for water solvation, the integral

equation formalism polarizable continuum model (IEFPCM) was used.

S2. Supporting Results

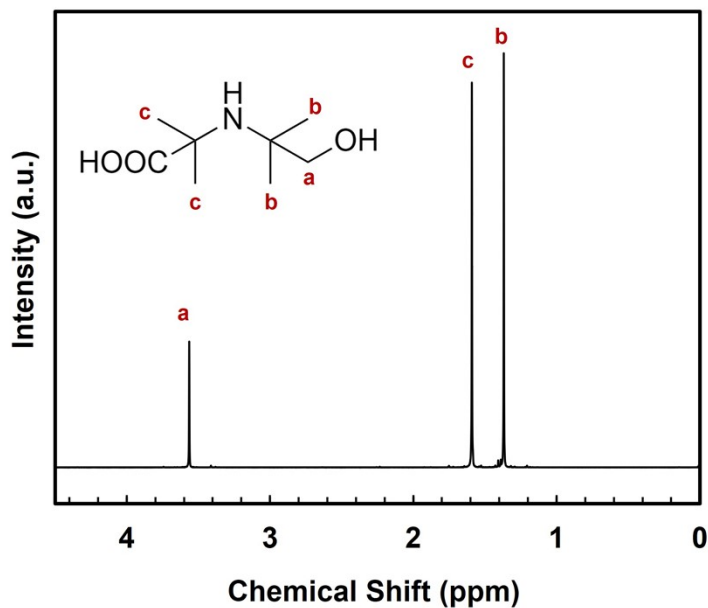


Figure S1. ¹H NMR spectrum of *N*-(1,1-dimethyl-2-hydroxyethyl)-aminoisobutyric acid.

Table S1. FTIR peak assignments for PVA/Gly membrane under humid CO₂ exposure.

Frequency [cm ⁻¹]	Assignment	Group	References
1615	$\nu_{\text{asym}}\text{COO}^-$	Carboxylate ion	[10–12]
1600	$\nu_{\text{asym}}\text{COO}^-$	Carbamate ion	[10–12]
1581	$\delta_{\text{asym}}\text{NH}_3^+$	Ammonium ion	[13,14]
1490	δNH	Carbamate ion	[10]
1470	$\delta_{\text{sym}}\text{NH}_3^+$	Ammonium ion	[13,14]
1400	$\nu_{\text{sym}}\text{COO}^-$	Carbamate	[10,11]
1355	$\nu_{\text{sym}}\text{COO}^-$	Carbamate	[10,11]
1335	νCN	Carbamate	[10,11]

Table S2. FTIR peak assignments for PVA/TB-AIBA membrane under humid CO₂ exposure

Frequency [cm ⁻¹]	Assignment	Group	References
1655	$\nu_{\text{asym}}\text{HCO}_3^-$	Bicarbonate	[10,15]
1250 – 1300	$\nu_{\text{sym}}\text{HCO}_3^-$	Bicarbonate	[10,15]

Table S3. H₂S/CO₂ separation performance of Gly-based FTM (3 μm thickness) at various H₂S concentrations.

H ₂ S conc. (vol.%)	H ₂ S permeance (GPU)	CO ₂ permeance (GPU)	H ₂ S/CO ₂ selectivity
1.4	217	67	3.2
2.6	191	53	3.6
4.1	200	49	4.1
7.7	185	45	4.1
10.8	161	43	3.7
12.6	184	47	3.9
14.4	165	39	4.2
16.7	179	42	4.3
20.3	179	47	3.8
22.4	170	44	3.9
25.3	145	37	3.9

Table S4. H₂S/CO₂ separation performance of TB-AIBA-based FTM (3 μm thickness) at various H₂S concentrations.

H ₂ S conc. (vol.%)	H ₂ S permeance (GPU)	CO ₂ permeance (GPU)	H ₂ S/CO ₂ selectivity
0.5	764	30	25.2
0.7	719	31	23.3
0.9	619	31	20.2
1.2	563	29	19.5
1.7	492	27	18
3.0	450	28	16.3
4.0	440	31	14.1
6.0	377	31	12.1
9.4	320	27	11.9
12.7	299	27	11.1
17.9	265	26	10.1
23.2	245	30	8.2
27.6	217	28	7.7

S3. Carrier Structures and Properties

Figure S2 (a) shows the chemical structures of some sterically hindered amines often used for absorption-based H₂S/CO₂ separation: 2-amino-2-methyl-1-propanol (2-AMP) and piperazine (PZ) [16–18]. The *N*-exposure parameter of each of these amines has been computed and contrasted with that of Gly and TB-AIBA [19]. As the name implies, the *N*-exposure parameter evaluates how much of the van der Waals surface of the nitrogen atom is exposed and provides a quantitative and unbiased measure of steric hindrance. Figure S2 (b) depicts the measurement of the *N*-exposure of glycinate. As seen in Figure S2 (c), TB-AIBA has a much higher degree of steric hindrance, i.e., lower *N*-exposure parameter, than the amines commonly used in absorption systems.

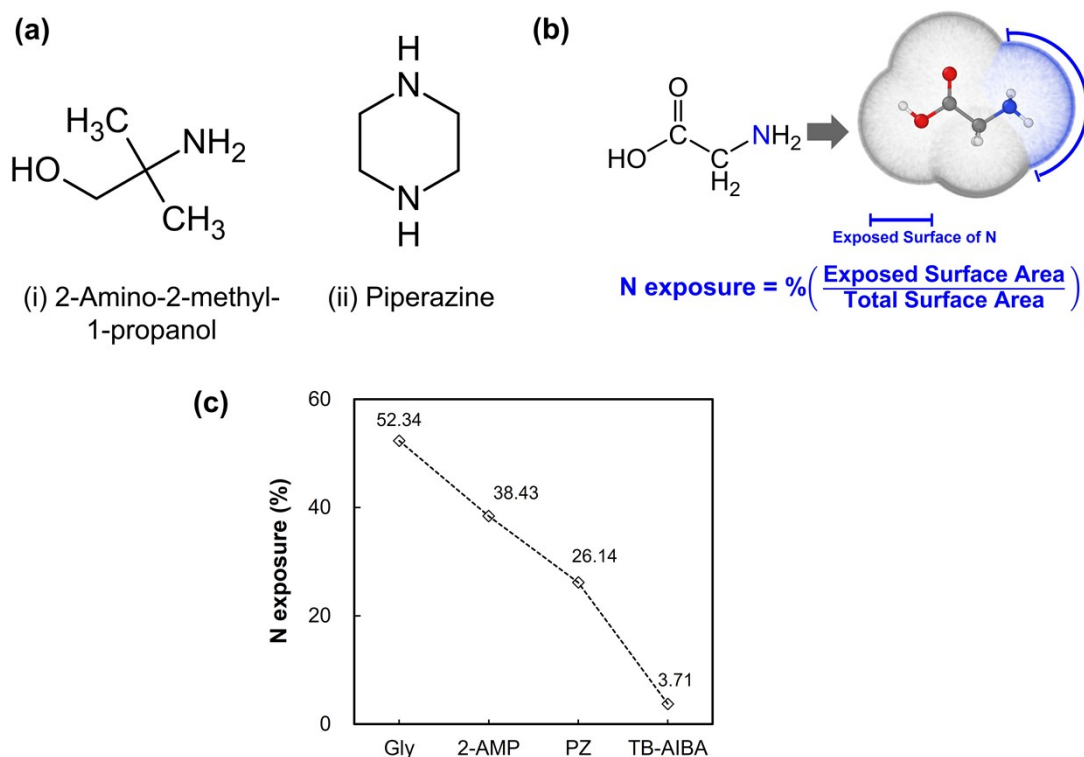


Figure S2. (a) Chemical structures of selected sterically hindered amines: (i) 2-AMP and (ii) PZ. (b) Graphical representation of the measurement of *N* exposure using the example of glycine. (c) *N* exposure values of selected sterically hindered amines, measured using a probe radius of 1 Å.

S4. Thickness-dependence of H₂S Permeability

The thickness-dependent permeability of FTMs is a well-reported phenomenon [7]. The acid gas molecules react with the carriers at the feed/membrane interface via a reversible reaction to form a reaction product. The product then releases the acid gas at the membrane/permeate interface through the reverse reaction. The mass transfer resistances at these interfaces, caused by the forward and reverse reactions, are independent of membrane thickness. As a result, the acid gas permeability varies non-linearly with thickness. For conventional CO₂/inert gas FTMs, the CO₂ permeability generally increases with membrane thickness [7]. This is because CO₂ transport is controlled by the interfacial reaction resistance. Upon increasing the thickness, the contribution of interfacial reaction resistances is diminished, leading to an increase in permeability[7].

However, for H₂S/CO₂ separation, the thickness-dependence is rather more complicated. The H₂S permeability goes through a maximum as the thickness is increased (see Table S5 for effect of thickness on permeability). Initially, as the thickness is increased up to ca. 10 μm, the H₂S permeability increases. In this range of thicknesses, competitive CO₂ facilitation is minimal. Accordingly, upon increasing the thickness, the effect of the interfacial reaction resistance is decreased and the H₂S permeability increases from 1857 to 5050 Barrer (see Table S5). However, upon further increasing the thickness, the amine carriers react preferentially with CO₂ rather than H₂S, causing a drop in the H₂S facilitation. Due to this, the H₂S permeability goes through a maximum as the thickness increases, leading to the unusual trend seen in Figure 3 (b).

Table S5. H₂S/CO₂ separation performance of Gly- and TB-AIBA-based FTMs of varying thickness.

Carrier	Thickness (μm)	H ₂ S/CO ₂ selectivity	H ₂ S permeance (GPU)	H ₂ S permeability (Barrer)
Gly	3	3.8	289	867
	20	4	173	3460
	40	2.7	102	4080
	55	1.6	59	3245
TB-AIBA	3	20.2	619	1857
	10	15.1	505	5050
	25	4.3	69	1725
	30	1.8	18	540

Figure S3 plots the H₂S/CO₂ selectivities of the Gly and TB-AIBA FTMs against the H₂S permeances. The H₂S/CO₂ separation performance of selected polymer and the upper bounds have been calculated assuming a membrane thickness of 3 μm. It should be mentioned that TB-AIBA FTMs with thickness below 3 μm were synthesized and tested over the course of this work. However, the FTMs were prone to leaks, causing performance deterioration during testing. This was attributed to the high degree of crystallinity and the poor mechanical properties of the thinner FTMs. Such problems can be resolved by the use of polymeric fixed site carriers such as sterically hindered polyamines, an approach that will be explored in the future.

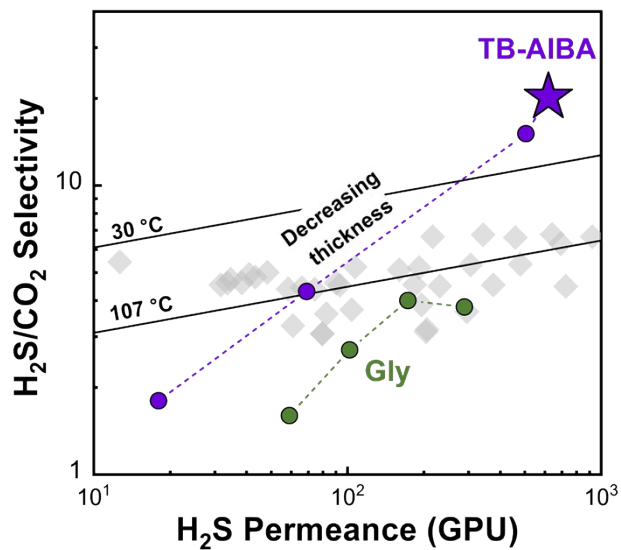


Figure S3. H₂S/CO₂ separation performances of TB-AIBA and Gly-based FTMs against selected literature data (represented by the grey markers) and the H₂S/CO₂ upper bounds (solid black lines) [20–28]. The H₂S permeance of literature data and the upper bounds have been calculated assuming a membrane thickness of 3 μm.

S5. Facilitated Transport Model

The reactions of sterically hindered amines with H₂S and CO₂ can be represented by Equation (4) and Equation (5), respectively [29]:



where R₁ and R₂ represent alkyl groups or a hydrogen atom.

The Damköhler number for the amine-H₂S reaction (D_a , defined as $D_a = \frac{k_r l^2}{D_{\text{HS}^-}}$, where k_r is the rate constant of the reverse reaction, l represents the membrane thickness, and D_{HS^-} stands for the diffusivity of the HS⁻ anion) is in the order of 10⁵ – 10⁶ [30]. The large value of D_a implies that the amine-H₂S reaction is at chemical equilibrium throughout the membrane. The equilibrium constant for the reaction, $K_{\text{H}_2\text{S}}$, is given by the equation:

$$K_{\text{H}_2\text{S}} = \frac{C_{\text{HS}^-} C_{\text{RNH}_3^+}}{C_{\text{H}_2\text{S}} C_{\text{RNH}_2}} \quad (6)$$

Although the amine-CO₂ reaction is not at equilibrium, it can be represented similarly:

$$K_{\text{CO}_2} = \frac{C_{\text{HCO}_3^-} C_{\text{RNH}_3^+}}{C_{\text{CO}_2} C_{\text{RNH}_2}} \quad (7)$$

where K_{CO_2} is the equilibrium constant for the reaction. Since the water sorption of the FTM is several times that of the CO₂ sorption, the water concentration is treated as a constant.

In addition to solution-diffusion permeation, H₂S and CO₂ will be transported across the membrane as HS⁻ and HCO₃⁻. The magnitude of this facilitated transport will be dependent on the total amine carrier concentration, C_T , which is given by:

$$C_T = C_{RNH_2} + C_{RNH_3^+} \quad (8)$$

Furthermore, electroneutrality demands that:

$$C_{RNH_3^+} = C_{HS^-} + C_{HCO_3^-} \quad (9)$$

Solving Equations (6) – (9) simultaneously, we can express the concentration of the hydrosulfide anion, C_{HS^-} , in terms of C_T , C_{H_2S} and C_{CO_2} :

$$C_{HS^-} = \frac{K_{H_2S}C_{H_2S}}{2} \left(\sqrt{1 + \frac{4C_T}{K_{H_2S}C_{H_2S} + K_{CO_2}C_{CO_2}}} - 1 \right) \quad (10)$$

Assuming that the H_2S partial pressure on the permeate side can be neglected, the H_2S flux of the FTM, J_{H_2S} , can be expressed as the sum of the non-reactive solution-diffusion flux, (transport as H_2S) and the facilitated transport as HS^- :

$$J_{H_2S} = D_{H_2S} \times [C_{H_2S} - 0] + D_{HS^-} \times [C_{HS^-} - 0] \quad (11)$$

The expression for C_{HS^-} from Equation (10) can be substituted into Equation (11). Further, Henry's law can be applied to obtain the expressions for C_{H_2S} and C_{CO_2} ($C_{H_2S} = H_{H_2S}p_{H_2S}$ and $C_{CO_2} = H_{CO_2}p_{CO_2}$, where H_{H_2S} and H_{CO_2} stand for the Henry's law constants of CO_2 and H_2S respectively, and p_{H_2S} and p_{CO_2} stand for the feed-side partial pressures of H_2S and CO_2 respectively). Then, dividing Equation (11) by the H_2S partial pressure driving force gives us the term for the H_2S permeance P_{H_2S} :

$$P_{H_2S} = P_{SD} + \frac{D_{HS^-}K_{H_2S}H_{H_2S}}{l} \left(\sqrt{1 + \frac{4C_T}{K_{H_2S}H_{H_2S}p_{H_2S} + K_{CO_2}H_{CO_2}p_{CO_2}}} - 1 \right) \quad (12)$$

where P_{SD} is the solution-diffusion permeance.

Some additional approximations are necessary to simplify Equation (12) for the purpose of a model-fitting. We assume that facilitated transport is the main contributor to the H_2S permeance,

and that P_{SD} can be neglected in comparison. This is particularly the case at 107°C, where the physical solubility of H₂S is further diminished compared to lower temperatures.

Furthermore, the significant contribution of facilitated transport suggests that the FTM is still far

from complete saturation. This suggests that $\frac{4C_T}{K_{H_2S}H_{H_2S}p_{H_2S} + K_{CO_2}H_{CO_2}p_{CO_2}} \gg 1$ [31]. Accordingly,

Equation (12) can be approximated as:

$$P_{H_2S} = \frac{D_{HS} - K_{H_2S}H_{H_2S}}{l} \left(\sqrt{\frac{4C_T}{K_{H_2S}H_{H_2S}p_{H_2S} + K_{CO_2}H_{CO_2}p_{CO_2}}} \right) \quad (13)$$

Then, upon lumping some terms and expressing p_{H_2S} and p_{CO_2} in terms of feed-side H₂S and CO₂ mole fractions x_{H_2S} and x_{CO_2} and the total pressure p , we get an equation of the form:

$$P_{H_2S} = \sqrt{\frac{1}{\gamma_{H_2S}x_{H_2S} + \gamma_{CO_2}x_{CO_2}}} \quad (14)$$

It is important to emphasize that the assumption of chemical equilibrium is not required for the mathematical formulation of the kinetically controlled H₂S/CO₂ selectivity. While detailed kinetic modelling is beyond the scope of this work, the impact of thickness on selectivity can be illustrated using the facilitated transport model developed by Dindi et al [32]. In their model, the facilitation factor (ratio of total flux to the solution-diffusion flux) of CO₂, F_{CO_2} , can be described by the equation:

$$F_{CO_2} = \frac{1 + \alpha_{CO_2}K_{CO_2}C_{RNH_2}}{1 + \alpha_{CO_2}K_{CO_2}C_{RNH_2} \times \frac{\tanh(\lambda_{CO_2})}{\lambda_{CO_2}}} \quad (15)$$

where C_{RNH_2} refers to the free amine concentration as above. K_{CO_2} refers to the equilibrium constant as defined in Equation (7). α_{CO_2} refers to the mobility ratio, defined as:

$$\alpha_{CO_2} = \frac{D_{HCO_3^-} C_{RNH_3^+}}{D_{CO_2} C_{RNH_2}} \quad (16)$$

λ_{CO_2} is defined as follows:

$$\lambda_{CO_2} = \sqrt{\frac{1 + \alpha_{CO_2} K_{CO_2} C_{RNH_2}}{\epsilon_{CO_2}}} \quad (17)$$

where ϵ is the inverse of the Damköhler number, defined here as:

$$\epsilon_{CO_2} = \frac{D_{HCO_3^-}}{k_{rCO_2} l^2} \quad (18)$$

k_{rCO_2} refers to the rate constant of the reverse reaction and l stands for the membrane thickness.

Likewise, a facilitation factor can be defined for the H_2S transport as well:

$$F_{H_2S} = \frac{1 + \alpha_{H_2S} K_{H_2S} C_{RNH_2}}{1 + \alpha_{H_2S} K_{H_2S} C_{RNH_2} \times \frac{\tanh(\lambda_{H_2S})}{\lambda_{H_2S}}} \quad (19)$$

The dimensionless variables are defined similarly to those in Equations. (16) – (18).

The H_2S reaction is nearly instantaneous, and thereby $k_{rH_2S} l^2 \gg D_{HS^-}$, regardless of the value of l . Accordingly, $\epsilon_{H_2S} \ll 1$ and $\lambda_{H_2S} \rightarrow \infty$. In the context of an instantaneous reaction, F_{H_2S} can be approximated as:

$$\lim_{\lambda_{H_2S} \rightarrow \infty} F_{H_2S} = 1 + \alpha_{H_2S} K_{H_2S} C_{RNH_2} \quad (20)$$

The CO_2 reaction, on the other hand, is significantly slower, and k_{rCO_2} is a smaller, finite value. Consequently, F_{CO_2} is strongly dependent on the membrane thickness, l . This can be illustrated by considering the two extreme cases: $l \rightarrow 0$ (an extremely thin membrane), and $l \rightarrow \infty$ (an extremely thick membrane).

For the ideal case of an extremely thin membrane, $l \rightarrow 0$ and $k_{rCO_2} l^2 \ll D_{HCO_3^-}$. Accordingly,

$\epsilon_{CO_2} \rightarrow \infty$ and $\lambda_{CO_2} \rightarrow 0$. $\frac{\tanh(\lambda_{CO_2})}{\lambda_{CO_2}} \rightarrow 1$, and the value of F_{CO_2} approaches 1, indicating that the CO_2 transport occurs only via the solution-diffusion mechanism. In this case, the facilitated transport of CO_2 is negligible, a condition that corresponds to kinetically controlled separation.

For the opposite scenario of an extremely thick membrane, $l \rightarrow \infty$ and $k_{rCO_2} l^2 \gg D_{HCO_3^-}$.

Accordingly, $\epsilon_{CO_2} \rightarrow 0$ and $\lambda_{CO_2} \rightarrow \infty$. $\frac{\tanh(\lambda_{CO_2})}{\lambda_{CO_2}} \rightarrow 0$, and F_{CO_2} is given by the equation:

$$\lim_{\lambda_{CO_2} \rightarrow \infty} F_{CO_2} = 1 + \alpha_{CO_2} K_{CO_2} C_{RNH_2} \quad (21)$$

This condition corresponds to thermodynamically controlled separation. There is significant competitive transport of CO_2 , which negatively affects the H_2S/CO_2 selectivity.

S6. H₂S/CO₂ Upper Bounds and Literature Data

As per Rowe et al., for a gas pair i and j , the upper bound is given by the equation [20]:

$$\alpha_{i/j} = \frac{\beta_{ij}}{P_i^{\lambda_{ij}}} \quad (22)$$

where λ_{ij} controls the slope of the upper bound and β_{ij} is the intercept. P_i refers to the permeability of gas species i , and $\alpha_{i/j}$ refers to the ideal selectivity between two gas species i and j . λ_{ij} can be related to the kinetic diameter d_i of the species i by the equation [20]:

$$\lambda_{ij} = \left(\frac{d_j}{d_i}\right)^2 - 1 \quad (23)$$

β_{ij} can be related to the solubility S_i of the gas species i in the polymer by the equation:

$$\beta_{ij} = \frac{S_i}{S_j} S_i^{\lambda_{ij}} \times \exp\left\{-\lambda_{ij}\left(b - f\left(\frac{1-a}{RT}\right)\right)\right\} \quad (24)$$

where a and b are parameters independent of gas type, and f serves as a measure of chain rigidity [20]. R refers to the universal gas constant, and T refers to the absolute temperature. S_i can be

related to the Lennard-Jones temperature $\frac{\varepsilon_i}{k}$ by the equation:

$$\ln S_i = M + N \frac{\varepsilon_i}{k} - \left(500 - 10 \frac{\varepsilon_i}{k}\right) \left(\frac{1}{T} - \frac{1}{298}\right) \quad (25)$$

where M is sensitive to the polymer and the gas species, and N takes a value of 0.023 K⁻¹ [20].

The values of d_i , a , b , f , M , N , and $\frac{\varepsilon_i}{k}$ used for drawing the upper bounds in Figure 3 (b) are given in Table S6.

Table S6. Parameters used for calculating the H₂S/CO₂ upper bounds [20,27].

Parameter	H ₂ S	CO ₂	Reference
d_i (Å)	3.6	3.3	[27]
ε_i/k (K)	301	195	
M	-9.84		[20]
N	0.023		
a	0.64		
b	11.5		
f (cal/mol)	0		

The H₂S/CO₂ separation performances of literature membranes, represented by grey markers in Figure 3 (b), are presented in Table S7.

Table S7. H₂S/CO₂ separation performances of selected polymers [22,23,26,28].

Material	H ₂ S permeability (Barrer)	H ₂ S/CO ₂ selectivity	References
Poly(ether urethanes)	239	3.1	[26]
PU1	183	3.3	
PU2	613	3.1	
	618	3.2	
PU3	271	4.6	
	280	4.5	
PU4	199	4.4	
	223	4.4	
	95	4.5	
	101	4.6	
	115	4.6	
	104	4.7	
	123	4.9	
Pebax MX series	130	4.8	
	695	4.5	
	553	4.5	
	248	3.6	
Pebax SA00	175	4.4	
	312	3.7	
	888	3.7	

	38	5.4	
	8	2.0	
Crosslinked PEO MW 200	0.07	1.0	
Crosslinked PEO MW 300	0.24	2.2	
Crosslinked PEO MW 400	0.50	2.5	
Crosslinked PEO MW 600	9.27	4.0	[23]
Crosslinked PEO MW 1000	25.94	5.0	
Crosslinked PEO MW 2050	2.95	4.3	
Polyphosphazene 1	14.1	1.9	
Polyphosphazene 2	588.0	3.9	[28]
Polyphosphazene 3	1130.0	4.5	
PA12-PEO-50	1030	6.7	
	1929	6.8	
	2775	6.6	
PA6-PEO-60	651	6.6	
	1380	6.6	
	2083	6.3	
PA12-PTMEO-80	2180	4.5	
	3567	4.2	[22]
	4713	3.7	
PA12-PEO-a-50	481	5.1	
	920	5.3	
	1444	5.3	
PA6-PTMEO-33	145	5.0	
	322	5.2	
	576	5.2	

S7. References

- [1] K. Zhang, B. B. Noble, A. C. Mater, M. J. Monteiro, M. L. Coote, Z. Jia, *Phys. Chem. Chem. Phys.* **2018**, *20*, 2606–2614.
- [2] S. D. Rychnovsky, T. Beauchamp, R. Vaidyanathan, T. Kwan, *J. Org. Chem.* **1998**, *63*, 6363–6374.
- [3] S. Rao, Y. Han, W. S. W. Ho, *J. Membr. Sci.* **2023**, *686*, 121989.
- [4] D. Wu, C. Sun, P. K. Dutta, W. S. W. Ho, *J. Membr. Sci.* **2017**, *534*, 33–45.
- [5] K. K. Chen, W. Salim, Y. Han, M. Gasda, W. S. W. Ho, *J. Membr. Sci.* **2020**, *612*, 118484.
- [6] R. Xing, W. S. W. Ho, *J. Membr. Sci.* **2011**, *367*, 91–102.
- [7] L. Ansaloni, Y. Zhao, B. T. Jung, K. Ramasubramanian, M. G. Baschetti, W. S. W. Ho, *J. Membr. Sci.* **2015**, *490*, 18–28.
- [8] P. R. Bevington, D. K. Robinson, J. M. Blair, A. J. Mallinckrodt, S. McKay, *Comput. Phys.* **1993**, *7*, 415–416.
- [9] X. Deng, C. Zou, Y. Han, L.-C. Lin, W. S. W. Ho, *J. Phys. Chem. C* **2020**, *124*, 25322–25330.
- [10] G. S. Foo, J. J. Lee, C. Chen, S. E. Hayes, C. Sievers, C. W. Jones, *ChemSusChem* **2017**, *10*, 266–276.
- [11] S. G. Pate, H. Xu, C. P. O’Brien, *J. Mater. Chem. A* **2022**, *10*, 4418–4427.
- [12] G. Latini, M. Signorile, V. Crocellà, S. Bocchini, C. F. Pirri, S. Bordiga, *Catal. Today* **2019**, *336*, 148–160.
- [13] W. C. Wilfong, C. S. Srikanth, S. S. C. Chuang, *ACS Appl. Mater. Interfaces* **2014**, *6*, 13617–13626.
- [14] D. D. Miller, S. S. C. Chuang, *J. Phys. Chem. C* **2016**, *120*, 25489–25504.
- [15] J. J. Lee, C.-J. Yoo, C.-H. Chen, S. E. Hayes, C. Sievers, C. W. Jones, *Langmuir* **2018**, *34*, 12279–12292.
- [16] A. K. Saha, S. S. Bandyopadhyay, P. Saju, A. K. Biswas, *Ind. Eng. Chem. Res.* **1993**, *32*, 3051–3055.
- [17] B. P. Mandal, A. K. Biswas, S. S. Bandyopadhyay, *Sep. Purif. Technol.* **2004**, *35*, 191–202.
- [18] W. Y. Lee, S. Y. Park, K. B. Lee, S. C. Nam, *Energy Fuels* **2020**, *34*, 1992–2000.
- [19] X. Deng, Y. Han, L.-C. Lin, W. S. W. Ho, *Sep. Purif. Technol.* **2022**, *299*, 121601.
- [20] B. W. Rowe, L. M. Robeson, B. D. Freeman, D. R. Paul, *J. Membr. Sci.* **2010**, *360*, 58–69.
- [21] C. A. Scholes, S. E. Kentish, G. W. Stevens, *Sep. Purif. Rev.* **2009**, *38*, 1–44.
- [22] D. J. Harrigan, J. Yang, B. J. Sundell, J. A. Lawrence, J. T. O’Brien, M. L. Ostraat, *J. Membr. Sci.* **2020**, *595*, 117497.
- [23] D. J. Harrigan, J. A. Lawrence, H. W. Reid, J. B. Rivers, J. T. O’Brien, S. A. Sharber, B. J. Sundell, *J. Membr. Sci.* **2020**, *602*, 117947.
- [24] Y. Ma, H. Guo, R. Selyanchyn, B. Wang, L. Deng, Z. Dai, X. Jiang, *J. Mater. Chem. A* **2021**, *9*, 20211–20240.
- [25] S. Rao, B. Prasad, Y. Han, W. S. W. Ho, *Energies* **2023**, *16*, 5713.
- [26] G. Chatterjee, A. A. Houde, S. A. Stern, *J. Membr. Sci.* **1997**, *135*, 99–106.
- [27] A. Hayek, Y. A. Shalabi, A. Alsamah, *Sep. Purif. Technol.* **2021**, *277*, 119535.
- [28] C. J. Orme, F. F. Stewart, *J. Membr. Sci.* **2005**, *253*, 243–249.
- [29] S. Li, Z. Wang, W. He, C. Zhang, H. Wu, J. Wang, S. Wang, *Ind. Eng. Chem. Res.* **2014**, *53*, 7758–7767.
- [30] J. D. Way, R. D. Noble, *J. Membr. Sci.* **1989**, *46*, 309–324.

- [31] F. Gioia, G. Astarita, *Ind. Eng. Chem. Fundam.* **1967**, 6, 370–375.
- [32] A. Dindi, R. D. Noble, C. A. Koval, *J. Membr. Sci.* **1992**, 65, 39–45.